Ab initio simulation of the electron energy-loss near-edge structures at the Li *K* edge in Li, Li_2O, and $LiMn_2O_4$

V. Mauchamp, F. Boucher, G. Ouvrard, and P. Moreau
Institut des Matériaux Jean Rouxel, UMR 6502, Université de Nantes—CNRS, 2, rue de la Houssinière 44322 Nantes Cedex, France
(Received 1 June 2006; published 6 September 2006)

Ab initio simulations of the electron energy-loss near edge structures (ELNES) at the Li *K* edge were obtained with the WIEN2k code, which is based on the density functional theory (DFT). Since the 1*s* states of the lithium atoms must be considered as semicore states, the standard procedure to calculate the dynamic form factor (DFF) has to be modified. The difficulties raised by the delocalized nature of these states and their influence on the simulated spectra are discussed. Unphysical monopolar transitions are shown to be extremely large and the description of the Li 1*s* orbital as a core or valence state for the self-consistent determination of potentials is proven to have little influence on the calculated spectrum shape. Comparisons between simulated and experimental spectra for three different compounds are presented: Li, Li_2O, and $LiMn_2O_4$ (a metal, an insulator, and a transition metal oxide). All simulations fit well the experiments, thus demonstrating that this approach can be applied to a wide range of lithiated compounds. In the case of the Li *K* edge in Li_2O, we also show that the recently proposed partition of the spectrum into two energy range regions, with different core hole strengths, improves the concordance between the simulation and the experiment. Finally, the influence of the real part of the dielectric function, omitted when using the DFF, is assessed. A comparison of Li *K* edges calculated using either the loss function $[\mathrm{Im}(-1/\varepsilon)]$ or only the DFF (imaginary part of ε) is presented in detail. We show that polarization effects are particularly strong in the Li *K* edge of $LiMn_2O_4$ due to the presence of the Mn $M_{2,3}$ edge. Other calculations including the GW approximation and the local field effects would, however, be necessary to precisely quantify these effects.

DOI: 10.1103/PhysRevB.74.115106 PACS number(s): 79.20.Uv, 71.20.Tx, 78.20.Ci, 82.80.Pv

I. INTRODUCTION

It has long been recognized that electron energy-loss spectroscopy (EELS) in a transmission electron microscope (TEM) can provide information of considerable chemical significance in the field of material science.[1] Such information can be retrieved from the natural partition between the low and high-loss regions of the spectrum, a partition which has prevailed since the early days of EELS. The low-loss region (from 0 eV to approximately 50 eV), where plasmon modes,[1] interband transitions and excitons in insulators appear,[2,3] can be used to characterize phases,[4] band gaps,[5,6] or interfaces.[7] Where possible, the results are compared with optical data and dielectric functions. The high-loss region (energy losses higher than 50 eV) usually gives similar results to x-ray absorption spectroscopy. It corresponds to electron excitations from core levels to unoccupied levels and is more frequently exploited than the low-loss region. Due to the highly localized interactions in the case of core-loss spectra,[1] the small probes now available in TEMs allow analyzes with unchallenged spatial resolution (sometimes better than 1 nm).[8] The core-loss spectra thus provide us with very local information on the following aspects: the anisotropy of chemical bonds,[9] the site symmetry via *d*-level splitting in transition metals,[10] the oxidation state of the excited atom,[11,12] or simply the composition. It comes as no surprise then that EELS has been widely used for the study of lithium battery electrodes, where local oxidation states and compositions are a critical matter. Most of the time, the focus is on the metal and oxygen edges (in oxide cathodes, for example), leading to new insights on the intercalation chemistry at work in the batteries.[13,14] Very few examples are to be found, however, in available literature on the study of the Li *K* edge in these materials. Even if, for instance, Graetz *et al.* probed this edge to check on the lithium content in their electrodes,[15] and Hightower *et al.* used it to show a very small lithium charge transfer in LiC_6 anodes,[16] the number of published results is nowhere near what one would expect considering the obvious essential role of lithium atoms in lithium batteries. The small number of studies of the Li *K* edge can partly be attributed to experimental difficulties, partly to theoretical uncertainties. For such a light element, radiation damages caused by the electron beam can be critical,[17] rendering the Li *K* edge hard to observe. Moreover, in lithium battery materials, the Li *K* edge is often superimposed onto the $M_{2,3}$ edge of a transition metal (V, Mn, Fe, …), leading to a difficult extraction of its intensity. On the theoretical side, the interpretation of the electron energy-loss near edge structures (ELNES) at the Li *K* edge is not straightforward and requires careful analysis. One could use the "finger print method," which consists in comparing the experimental spectrum with that of reference compounds. This method was successfully used by Shiraishi *et al.* to determine the oxidation states of Co, Cr, and Ni atoms in $LiMn_{1.6}M_{0.4}O_4$ (M=Co, Cr, Ni) from their $L_{2,3}$ edges.[18] However, this method becomes questionable when light atoms (i.e., with few electrons) inserted in a host matrix are considered. In such cases, their edges strongly depend on the electronic structure of the matrix. The interpretation of the Li *K* edge in Li battery electrodes thus requires theoretical simulations.

It may well be worth mentioning at this stage that the lithium *K* edge appears around 57 eV (±3 eV depending on its oxidation state). This position, somewhere around the

arbitrary limit between the low- and high-loss regions, explains why compounds containing lithium were theoretically approached from two different angles. Dielectric function theories were used to assess the importance of local field effects (LFE),[19] Zone boundary collective states,[20] and plasmon dispersion in the low energy-loss region.[21] Computer programs dedicated to the simulation of core losses were independently used to investigate core-hole effects on the lithium K edge in insulators using the $Z+1$ approximation.[22,23] This mutual exclusion between the two communities is not satisfactory and some assumptions which were made in the simulations should be clearly addressed. If one is to accurately simulate the EELS lithium K edge in lithium batteries, a study integrating and discussing both approaches is necessary. So, in order to do just this, we present simulations of Li K edges using the WIEN2k program,[24] a full potential linearized augmented plane wave (FLAPW) code,[25,26] based on the density functional theory (DFT).[27,28] This code has the advantage of allowing the simulation of this special edge, either by calculating the dynamic form factor (DFF),[29] or by working within the dielectric function framework.[30] Since conclusions may vary as a function of the kind of material considered, we chose two simple compounds, Li metal and Li_2O, to assess the influence of the conducting properties on the simulation, and $LiMn_2O_4$ in order to address the problem of the presence of a transition metal $M_{2,3}$ edge just before the Li K edge.

In this paper we first present the conditions used to acquire the experimental spectra and then go on to address the relevant computational manipulations in order to obtain the DFF. We pay particular attention to the difficulties raised by the delocalized nature of the Li 1s core states and discuss the effect these have on the shape of simulated Li K edges. Simulations and experimental spectra obtained on $LiMn_2O_4$, Li_2O and pure Li are then compared in order to illustrate the strengths and weaknesses of this DFF method. Last, the polarization effects on the Li K edge in $LiMn_2O_4$ are put forward and examined in order to favor improved simulations of EELS spectra in the case of lithium battery materials.

II. EXPERIMENT

$LiMn_2O_4$ was synthesized by a solid-state reaction in air starting with Li_2CO_3 (Prolabo Rectapur 99%) and $MnCO_3$ (Aldrich 99.9%) first at 900 K for decarbonation, then at 1073 K (for 20 h), after having ground the powder carefully. The x-ray diffraction diagram of the powder showed that the cubic phase was obtained. The Li_2O powder was purchased from Alpha Aesar (99.5% purity). This sample was prepared under an inert argon atmosphere in a glove box. Powders were crushed in hexane, deposited onto a holey carbon grid and then inserted into a GATAN 648 vacuum transfer sample holder. Prior to its introduction into the microscope, the sample holder containing the sample was placed under vacuum at 100 °C to remove surface contamination. The Li metal sample was also prepared in a glove box by cutting a thin slab from a lithium foil (99.9%, Alpha Aesar), after which it was placed directly into the vacuum sample holder and inserted into the microscope. In spite of all these precautions, most observed areas were slightly oxidized. However, as already mentioned by Liu *et al.*,[31] pure lithium crystals grow not far from where the beam is focussed and we collected our lithium spectra from these crystals.

Experiments were performed with a TEM-field emission gun (FEG) Hitachi HF 2000 operated at 100 kV, and spectra were recorded using a GATAN 666 parallel spectrometer. The energy resolution given by the zero loss peak (ZLP) full width at half maximum was 0.9 eV with a dispersion of 0.2 eV/channel. All spectra were dark count corrected. Convergence and acceptance angles were respectively 1.4 mrad and 18.2 mrad. In order to avoid irradiation damages, an uncondensed 400 nm diameter probe was used. Total acquisition times were 2.5 s and 0.25 s for the Li K edge (50–200 eV) and the low-loss region (0–150 eV), respectively. After acquisition, the spectra were first deconvolved by the ZLP with the PEELS program.[32] A tied background was then subtracted from the ELNES spectra using a power law. The utilization of a tied background gave very satisfactory results,[33] with intensities in the first 20 eV after the edge onsets hardly dependant on the chosen energy windows. Where possible, multiple scattering was removed from the low-loss spectra following Stephen's procedure.[34]

III. COMPUTATIONAL ASPECTS FOR THE DFF SIMULATION OF THE LI K EDGE

Calculations were all carried out within the general gradient approximation (GGA) using Perdew, Burke, and Ernzerhof's exchange and correlation potential.[35]

A. LAPW method: treatment of semicore states

LAPW methods are based on the use of a double basis set to describe Kohn-Sham wave functions of valence electrons.[25,26] The space is thus divided into two regions: the muffin tin (MT) region which consists of nonoverlapping spheres centered on each atom, and the interstitial region (IR) between the MT spheres. In the MT sphere, Kohn-Sham wave functions are developed on a linear combination of radial functions multiplied by spherical harmonics, whereas in the IR plane waves are used. This alternative to a pure plane waves basis set was first proposed by Slater in order to take the highly variable electronic density around the nuclei into account.[36] Based upon this partition of space, three distinct types of electronic orbitals are considered: (i) core states which are confined in the MT and do not participate directly in the chemical bonds with other atoms, (ii) valence states which leak out of the MT sphere and do participate in the chemical bonds, and (iii) semicore states which are extended core states (not fully confined in the MT sphere). The latter states, not very deep in energy, require a treatment similar to the one used for valence states. For linearized methods, the description of the semicore states is an issue. It frequently involves the treatment of two valence bands of the same azimuthal quantum number which lie in two different energy windows (for instance, 1s and 2s orbitals in the case of Li). Singh showed that the inclusion of localized orbitals in the MT sphere could solve this problem.[37] This treatment,

called (L)APW+LO, is now implemented in WIEN2k and provides excellent results. This approach was thus used in our calculations to describe lithium 1*s* semicore states. The description of these states, however, raises other complications as far as ELNES simulations are concerned. The following paragraph of this paper describes the basis of a standard ELNES calculation.

B. ELNES simulations

In the WIEN2k package, the TELNES program allows the simulation of EELS core losses and especially ELNES. In order to perform such simulations, it is necessary to evaluate the inelastic scattering cross section of a fast electron with the material. The doubly differential scattering cross section is, in the first Born approximation,[29] and considering independent particles,[38] proportional to the DFF given by

$$S(E,\vec{q}) \propto \sum_{i,f} |\langle \Psi_i | e^{i\vec{q}.\vec{r}} | \Psi_f \rangle|^2 \delta(E - E_f + E_i), \qquad (1)$$

where Ψ_i stands for the initial state of the wave function,Ψ_f for the final state (i.e., the excited state), $\vec{q}$ for the momentum transfer between the fast electron and the excited electron of the material, E for the energy-loss and E_f and E_i for the energy of the final and initial states, respectively. The Dirac function ensures energy conservation during the excitation process. Let it be noted that our convergent and collections angles are rather large. In order to avoid beam damages on these lithium based compounds, we also had to analyze large polycrystalline areas, so that the mixed dynamic form factor can safely be approximated by the DFF.[39,40] The calculation of the DFF with Eq. (1) is performed by the TELNES program using the method described by Nelhiebel *et al.*[41] In this method, the interaction operator $e^{i\vec{q}.\vec{r}}$ is expanded into spherical harmonics, i.e.

$$e^{i\vec{q}.\vec{r}} = 4\pi \sum_{\lambda=0}^{\infty} \sum_{\mu=-\lambda}^{+\lambda} i^{\lambda} Y_{\mu}^{\lambda}(\vec{q})^* Y_{\mu}^{\lambda}(\vec{r}) j_{\lambda}(q \,.\, r), \qquad (2)$$

where $\vec{q}=\vec{q}/q$, $\vec{r}=\vec{r}/r$, and $j_\lambda(x)$ is the spherical Bessel function of order λ. In our calculations, the matrix elements of the DFF were calculated expending $e^{i\vec{q}.\vec{r}}$ up to a λ value of 4. After having obtain a self-consistent potential, Kohn-Sham energies (eigenvalues) and Kohn-Sham wave functions (eigenvectors) necessary to evaluate the DFF were calculated over a large energy range going from −6.0 to 5.0 Ry. Convergence and acceptance angles were taken into account and the spectra obtained with TELNES were convolved with an energy-dependant Lorentzian function to get proper lifetime broadenings.[42] Since TELNES simulates core-loss spectra, the initial state Ψ_i has to be described as a core state. Consequently, the matrix elements of the DFF are calculated using only the expressions of the wave functions inside the MT sphere. This truncation raises problems for the simulation of low-lying edges, where the transition occurs from a semicore state which is not fully confined in the MT sphere, as to be seen in the case of the Li 1*s* state.

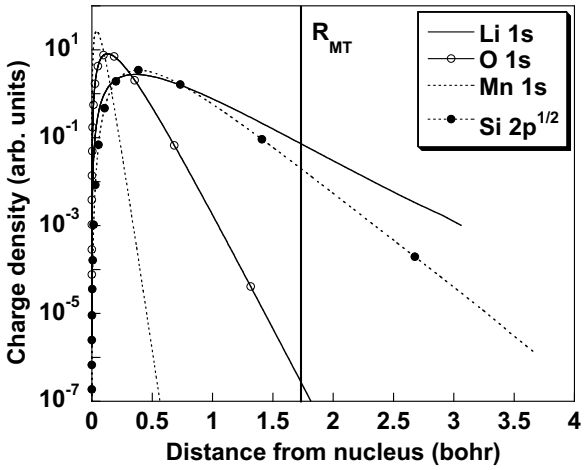

FIG. 1. Orbital charge densities as a function of the distance to the nucleus in $LiMn_2O_4$ and in Si. Full line for the 1s of Li; dotted line for the 1s of Mn; full line with open circles for the 1*s* of O; dotted line with full circles for the $2p^{1/2}$ of Si. The R_{MT} for Li (1.70 Bohr) is indicated by a vertical line.

C. Simulation of low-lying edges: limits of the MT approach

The problem of confinement within the MT spheres has already been discussed by Hébert *et al.* for the silicon *L* edge and Boron *K* edge.[43,44] Using the TELNES package, they showed that, wrong orthogonalization between Ψ_i, when described as a core state, and excited states of the same angular momentum quantum number, led to the calculation of an unphysical monopolar term in the simulated ELNES spectra. This orthogonalization is not provided numerically since the "real" Ψ_i state is not confined within the MT sphere. For fairly localized core states such as Boron 1*s* states, increasing the MT sphere radius (R_{MT}) allows for the recovery of a good orthogonalization between the different wave functions and thus avoiding this spurious monopolar contribution. However, in other more critical cases such as transitions from the Si 2*p* states, the monopolar part has to be systematically calculated and removed from the originally calculated spectrum. In fact, this contribution can account for a significant portion of the calculated spectrum (1/3rd in the case of silicon).[43] This effect should be even larger in lithium *K* edge simulations since the lithium 1*s* state is weakly bound to the nucleus. In Fig. 1, the radial distributions of the charge densities corresponding to the 1*s* states of lithium, manganese and oxygen atoms in the $LiMn_2O_4$ spinel compound and to the Si $2p^{1/2}$ states, are presented for comparison. All data concerning calculation parameters are given in Table I. Manganese and oxygen 1*s* states are clearly confined within the MT spheres, thereby leading to inexistent monopolar contributions in the calculation of their respective *K* edges. Such is not the case for Si $2p^{1/2}$ states, and even less so for the lithium 1*s* state. In the case of ELNES calculations, the monopolar part is thus an important issue and should not be included in the final spectrum. Taking different R_{MT} for the Li atom into consideration, the respective Li *K* edges in $LiMn_2O_4$ (without the monopolar term), as well as the monopolar contributions, are shown in Fig. 2. The same plane wave basis set was used for the four calculations in the

TABLE I. Parameters for the calculation of the ground states and the spectra using either TELNES or OPTIC programs in the case of Li, Li_2O, and $LiMn_2O_4$. All lengths given in Bohr units. For Li and Li_2O, nonconventional symmetries were used in order to isolate one Li atom. In the case of Li_2O with a core-hole, a $2\times2\times2$ unit cell was used in order to avoid interactions between adjacent core-holes. In the "*k* points" columns, the numbers refer to the sampling of the full Brillouin Zone.

	SCF cycles			TELNES		OPTIC	Cell	Cell
	k points	RK_{max}	R_{MT} Li	*k* points	Core hole	*k* points	parameter	symmetry
Li	$17\times17\times17$	7.0	2.85	$6\times6\times6$	No	$27\times27\times27$	6.63	$P4\bar{3}m$
Li_2O	$12\times12\times12$	7.0	1.70	$6\times6\times6$	No	$10\times10\times10$	8.73	$P\bar{4}3m$
Li_2O $(2\times2\times2)$	$6\times6\times6$	6.5	1.70	$5\times5\times5$	Yes		17.46	$P\bar{4}3m$
$LiMn_2O_4$	$10\times10\times10$	7.5	1.70	$6\times6\times6$	No	$11\times11\times11$	15.58	$Fd\bar{3}m$

interstitial region by setting the oxygen atom (R_{MT} = 1.55 bohr) as the smallest R_{MT}. The monopolar term (see inset of Fig. 2) can represent as much as 80% of the raw spectrum intensity for the smallest R_{MT}. Generally speaking, the larger the R_{MT}, the smaller the monopolar contribution. Shifting our focus to the simulated spectra, major differences were observed in the absolute intensities. We found that the larger the R_{MT} is, the larger the resulting calculated intensity. To facilitate the comparison, all calculated spectra were normalized at 13 eV. It was noted that up to 25 eV above threshold (Fig. 2), the relative intensities are practically the same and that the ELNES interpretation should not be impaired in that energy range. On the other hand, comparison between peaks situated too far apart might be less reliable since the relative intensities close to and far from the edge onset differ with increasing R_{MT}. These variations are not due to the calculation of the monopolar term since similar

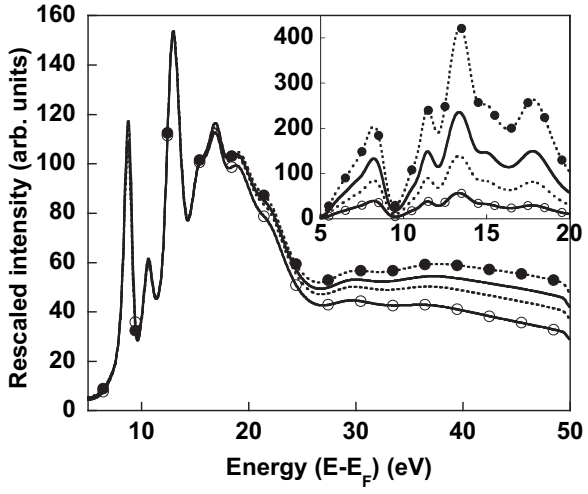

FIG. 2. Li K edge calculated in $LiMn_2O_4$, without the monopolar term and for different R_{MT}. Dotted line with full circles for R_{MT}=1.55 Bohr; full line for R_{MT}=1.70 Bohr; dotted line for R_{MT}=1.85 Bohr; full line with open circles for R_{MT} =2.10 Bohr. For comparison, the last three spectra were multiplied by 0.80, 0.68, and 0.55, respectively. The inset shows the corresponding monopolar terms for each of these radii (not rescaled).

calculation on the Na *K* edge in Na_2O, where the monopolar term is negligible, showed the same dependency on the R_{MT}. A similar evolution was also observed on the silicon *L* edge but was not discussed.[43] The choice of the muffin tin radii is thus critical in the description of transitions to high energy unoccupied states and its influence on the simulated spectra could be considered as a drawback with regards to the MT approach.

Having assessed the limits of the MT approach for low-energy edges, it appears that the Li *K* edge simulation raises another complication, as will be shown in the next paragraph.

D. Calculation of the DFF for the Li *K* edge

In the case of the lithium atom, the 1*s* state is so weakly bound to the nucleus that it is usually not treated as a core state but rather as a semicore one during the self-consistent determination of the electronic density. The DFF cannot then be directly evaluated with TELNES since, in this program, Ψ_i (the 1*s* Li state) is supposed to be described as a core state. To circumvent this problem, two types of approximation can be used. In an initial approach, different basis sets were used for the self-consistent field (SCF) cycle and the matrix element calculation. The 1*s* state of the excited Li is treated as a semicore (sc) state during the SCF determination of the electronic density (to be called SCF^{sc}) and a core state description is used afterwards to evaluate the DFF. No approximation is thus made on the density and the potential, but the basis set used to calculate the DFF is not perfectly adapted to this potential. When one then goes further to introduce a core-hole (ch) within this approach (to be called $SCF^{sc\text{-}ch}$), extensive file manipulations are needed in order to partially occupy the semicore band of the considered Li atom.

In another and much simpler approach, the same basis set can be used for the whole calculation: the Li 1*s* state can be described as a core state as early as the self-consistent determination of the electronic density (called SCF^{c}), the DFF can then straightforwardly be evaluated by TELNES from the corresponding Kohn-Sham energies. The introduction of a core hole is also particularly simple if desired (then called $SCF^{c\text{-}ch}$). In this method, however, an approximation is made

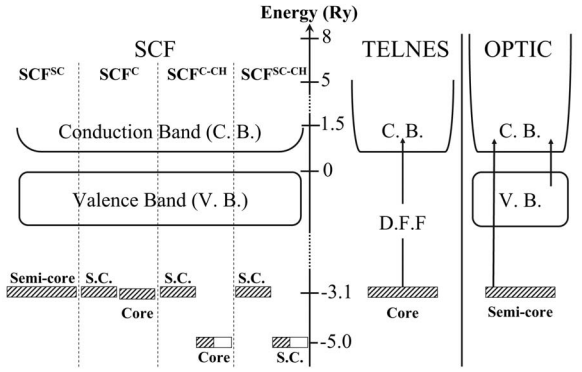

FIG. 3. Diagram summing up the different calculations used in this paper. On the left-hand side, the four approaches to calculate self-consistently the electronic density are represented: SCF^{sc} (Li 1*s* orbital in valence), SCF^{c} (Li 1*s* in core), $SCF^{c\text{-}ch}$ (Li 1*s* in core with one electron removed) and $SCF^{sc\text{-}ch}$ (Li 1*s* in valence with one electron removed). On the right hand side, the two methods used to calculate the Li *K* edge. TELNES: evaluation of the DFF between a core state and the Conduction Band (CB); OPTIC: evaluation of the imaginary part of the dielectric function by summing independent transitions between the valence band and the CB.

on the SCF density and potential with respect to the first method: the 1*s* charge leaking out of the MT sphere of the Li atom is not taken into account during the SCF cycles. It is therefore important to assess the influence of the treatment of the 1*s* state (either core or semicore) on the resulting *K* edge spectrum. The four possible choices (SCF^{sc}, SCF^{c}, $SCF^{sc\text{-}ch}$, $SCF^{c\text{-}ch}$), when performing the SCF determination of the electronic density, are presented on the left-hand side of Fig. 3. The Li 1*s* levels are represented by half-hatched or hatched rectangles, whether a core hole is included or not. As expected, from screening considerations, the introduction of a core-hole lowers the energy of the Li 1*s* orbital from −3.1 to −5 Ry with respect to the Fermi level. Having performed the SCF cycles, the lithium *K* edge can either be obtained from the DFF using the TELNES program (transitions from core levels to empty levels) or by calculating the dielectric function using the OPTIC program (transitions from the valence band to the conduction band). The OPTIC program results will be extensively discussed in Sec. V, once we have elaborated on the influence of the SCF approaches on the TELNES results.

First of all, differences induced by the SCF^{c} determination of the potentials with respect to the "exact" SCF^{sc} treatment are shown in Fig. 4 in the case of Li_2O. In order to isolate one Li atom in the unit cell, the symmetry was lowered from the usual $Fm\bar{3}m$ to the $P\bar{4}3m$ space group symmetry (see unit cell in Fig. 4). All four calculations were performed by focusing on the lithium atom in the $(\frac{1}{2},\frac{1}{2},\frac{1}{2})$ site. The total potential is shown along the $(x,\frac{1}{2},\frac{1}{2})$ line $(0 \leqslant x \leqslant 1)$ represented by an arrow in the atomic structure drawing. Since both SCF^{c} and SCF^{sc} potentials are extremely close to one another, the difference between the two is given in the upper panel of Fig. 4. Some discrepancies appear around the sphere boundary of the particularized Li but these variations have very small amplitudes with respect to the potential values. It

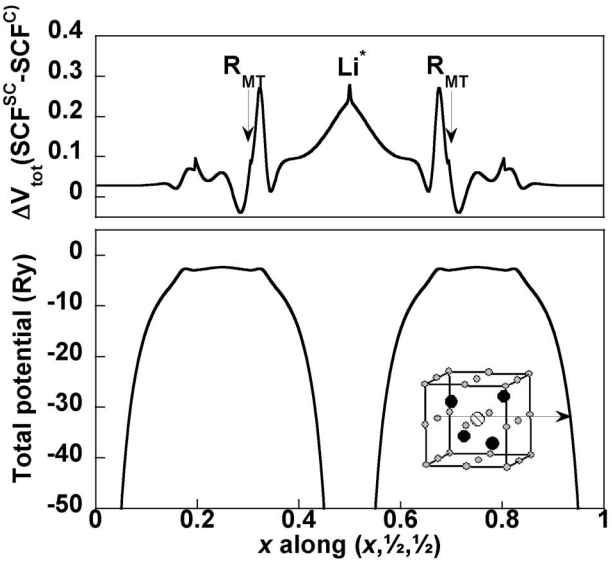

FIG. 4. Lower panel: total potential calculated along the $(x,\frac{1}{2},\frac{1}{2})$ line $(0 \leqslant x \leqslant 1)$ in the Li_2O unit cell. Upper panel: difference between the potentials obtained with the central Li atom treated using either the SCF^{sc} or the SCF^{c} method. The MT sphere boundaries of the central Li atom are indicated by arrows. The inset shows the Li_2O unit cell. Black spheres for oxygen atoms; grey spheres for Li atoms; stripped sphere for the central Li atom treated using either the SCF^{sc} or the SCF^{c} method.

is then not surprising that certain minor consequences are to be found on the resulting Li *K* edge simulations, as shown in Fig. 5(a). Since the presence of a core-hole tends to concentrate the electronic density in the MT sphere, the spectra obtained from the $SCF^{c\text{-}ch}$ and $SCF^{sc\text{-}ch}$ approaches [Fig. 5(b)] are even closer to each other than those obtained from the SCF^{c} and SCF^{sc} methods. Let it be noted that for the core-hole calculations, similarly to Jiang *et al.*,[23] we used a $(2a \times 2a \times 2a)$ supercell to avoid interactions between adjacent holes. The convergence of the calculation with respect to the supercell size was checked by calculating the lithium partial density of states.[45]

Consequently, as far as TELNES simulations are concerned, the cumbersome SCF^{sc} approaches (with or without a core hole) can reliably be replaced by the SCF^{c} ones (with or without a core hole, respectively). Having identified the most accurate and practical methods to calculate the Li *K* edge, the resulting theoretical spectra are compared to experimental ones in the next section.

IV. COMPARISON BETWEEN DFF SIMULATIONS AND EXPERIMENTAL SPECTRA

The results obtained on Li, $LiMn_2O_4$, and Li_2O are presented in Fig. 6(a)–6(c), respectively. The simulated spectra were shifted in energy, based on a visual match to the major feature of each experimental spectrum: the peaks at 56 eV, 65 eV, and 63.5 eV for Li, $LiMn_2O_4$, and Li_2O, respectively. In the case of Li_2O, which is a wide gap insulator (optical gap ~8 eV),[46] a core hole was introduced based on the gen-

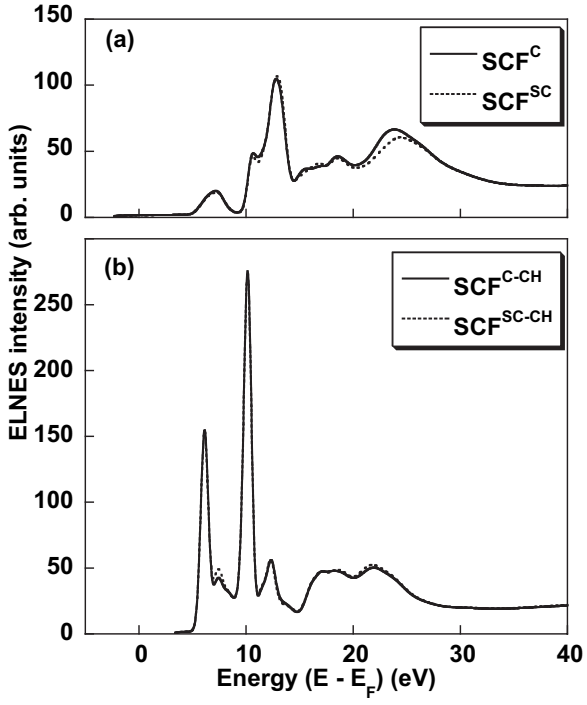

FIG. 5. Comparisons between simulated Li *K* edges in Li_2O. Full line for SCF^c calculations; dotted line for SCF^{sc} calculations. Calculations presented considering (a) no core-hole and (b) one core-hole.

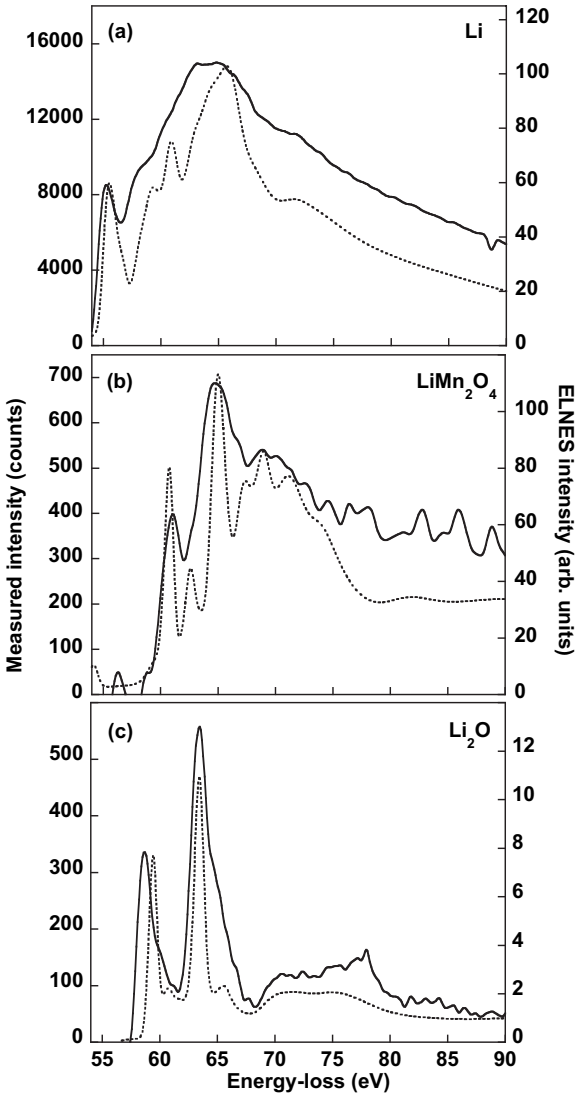

FIG. 6. Li *K* edge experiments and simulations for (a) Li, (b) $LiMn_2O_4$, and (c) Li_2O. Full lines: experiments; dotted lines: simulations. In the case of Li_2O, a core-hole in a supercell ($2a \times 2a \times 2a$) was introduced in the simulation.

eral opinion that core-hole effects are significant in insulating materials, whereas they can be neglected in metallic ones. In the case of Li, the overall agreement between experiment and simulation is good. The width of the main feature around 65 eV is underestimated when compared to the experiment but the calculated intensities of the first 10 eV reproduce the experiment fairly well. The simulation for $LiMn_2O_4$ [Fig. 6(b)] fits the relative positions of the different experimental features, namely the peaks at 60.7 and 65 eV as well as the broad features between 67.5 and 75 eV. Focussing on the relative intensities, one can observe some discrepancies on the intensity ratio between the peaks at 60.7 eV and 65 eV, as well as on the intensity around 70 eV. Where the latter difference, observed for all three compounds, could be due to either the choice of muffin tin radius (as was shown in the previous section) or to the type of power law used to remove the experimental background, the former one cannot. A possible explanation for this discrepancy will be given in the next section. In Fig. 6(c), the theoretical simulation of the Li *K* edge in Li_2O shows a strong concordance with the experimental spectrum. The splitting between the two first peaks is however a little bit underestimated, as already observed using the $Z+1$ approximation.[23] Their relative intensities are also not perfectly reproduced. Finally, within the broad feature between 70 and 80 eV, the intensity around 78 eV is significantly different. At this point we would like to stress that, since EELS involves electronic excitations, EELS spectra cannot be rigorously described within the framework of the DFT. The DFT considers independent particles and does not involve a time-depend perturbing field. The resolution of the Bethe-Salpeter equation provides the only accurate theoretical solution but this calculation is very time consuming.[47] It is for this reason that the core-hole effects on empty bands are taken into account artificially by self-consistently recalculating the electronic density after the removal of a core electron. This relies upon the screening of the core hole by the electronic density surrounding it. The simulations with one core-hole and without a core-hole are compared to the experiment in Fig. 7. When a core-hole is considered, the agreement is very good over the first 15 eV of the spectrum. The intensity around 78 eV is however not well reproduced. As already mentioned by Muller *et al.*,[48] the effect of the core-hole on empty states is energy dependant and should decrease as the excited electron kinetic energy increases. This explains why the accordance with experiment is better for the simulation without a core-hole than for that with a core-hole around 78 eV (high energy part of the Li_2O spectrum). Moreover, focussing on the inset, the transfer of the spectral weight to lower energies when a core-hole is in-

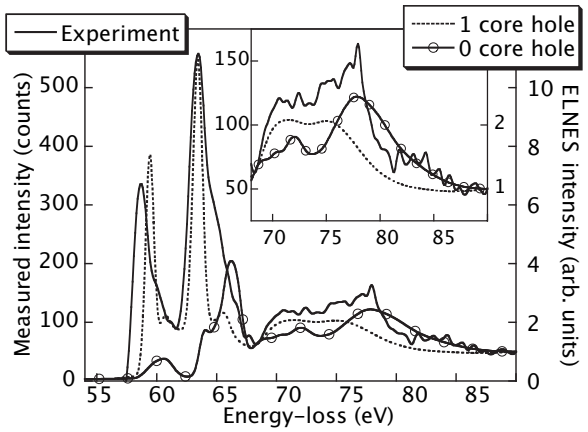

FIG. 7. Experimental and calculated Li *K* edges for Li_2O. Full line: experiment; dotted line: simulation by evaluating the DFF including a core-hole; full line with circles: simulation by evaluating the DFF without a core-hole. Inset: enlargement of the region between 65 and 90 eV. All spectrum intensities normalized at 90 eV.

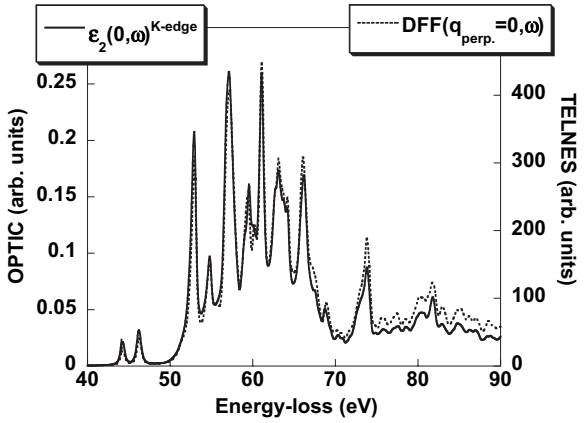

FIG. 8. Calculated Li *K* edges in $LiMn_2O_4$. Full line: calculation of $\varepsilon_2(0,\omega)$ using OPTIC program; dotted line: calculation of the DFF using TELNES program. In order to obtain a proper comparison, neither an integration over momentum transfer nor an energy-dependant lifetime broadening were considered for the calculation of the DFF. A constant broadening of 0.4 eV was applied in both cases.

cluded is in accordance with an overestimated attractive potential in this energy range. This energy dependence of the core-hole effect was already exemplified by Moreau *et al.* on totally different compounds (graphite, BN),[42] which demonstrates the practical validity of this method and a reasonable degree of generality.

In this section, we showed that the calculation of the DFF led to reasonable correlations with the experimental spectra, correlations that can be improved, if necessary, by the introduction of a core-hole (possibly partial). Some discrepancies can however be observed, in the case of $LiMn_2O_4$ for instance. It therefore warrants examining whether the omission of polarization effects (ε_1 in the dielectric function) could be responsible for these discrepancies. In order to answer this question, in the next section, we calculated the full dielectric function using the OPTIC program available in the WIEN2k package.

V. INFLUENCE OF THE REAL PART OF EPSILON

The OPTIC program calculates the dielectric function of a material, i.e., $\varepsilon(q=0,\omega)=\varepsilon_1+i\varepsilon_2$, in the random phase approximation (RPA) using the expression of the independent particle polarizability given by Hedin.[49] The code is based on the scheme developed by Ambrosh-Draxl and Sofo.[30] $\varepsilon_2(0,\omega)$ is determined via the calculation of matrix elements given by

$$M_i = \langle \Psi_i | \vec{p} \,.\, \vec{e}_i | \Psi_f \rangle, \tag{3}$$

where $\vec{p}$ is the polarization vector of the perturbing electromagnetic field. This expression is equivalent to Eq. (1) when considering the dipole approximation [valid for very small q in Eq. (1)] and a momentum transfer $\vec{q}=\vec{0}$; comparison between both calculations is thus legitimate. The real part of $\varepsilon(0,\omega)$ is then deduced from $\varepsilon_2(0,\omega)$ via a Kramers-Kronig analysis. In this method, the complete inversion of the dielectric matrix is not provided to obtain the loss function, so that local field effects (LFE) are not taken into account. Since this program was developed for calculations involving small transition energies (typically from 0 to 50 eV), Ψ_i is assumed to be a valence state (see the left panel of Fig. 3). Therefore, the Li 1*s* orbital is treated as a semicore state for the calculation of the excitation spectrum.

This OPTIC approach is very useful for two reasons. First of all, it provides another way of calculating matrix elements [as opposed to using TELNES, Eq. (1)] considering the Li 1*s* as a semicore state. Second, it also allows the calculation of $\varepsilon_1(0,\omega)$, a result essential to the rigorous simulation of the Li *K* edge, as will be shown in the next paragraph. In Fig. 8, the Li *K* edge obtained using the TELNES program [Eq. (1)] and $\varepsilon_2(0,\omega)$ considering only transitions from the Li 1*s* states using the OPTIC program [Eq. (3)], are compared in the case of $LiMn_2O_4$. The details of the latter calculation will be given in the following paragraphs. In order to provide a relevant comparison, the TELNES calculation was carried out considering both convergence and collection angles equal to 0 and a constant broadening of 0.4 eV. The two results are extremely similar. The small discrepancies between peak intensities are mainly due to slightly different matrix elements in [Eqs. (1) and (3)]. In fact, only the part of the wave function which is localized inside the muffin tin sphere is considered in TELNES, whereas in OPTIC, the entire wave function is used. Let it also be noted that in the OPTIC calculation, the monopolar term is nil since the entire Li 1*s* wave function is used to evaluate the matrix elements. The perfect match between both approaches (DFF and RPA) confirms that monopolar terms do not constitute a major problem as long as they are not taken into account in the final TELNES spectrum.

It is however well known that the EELS spectrum is rigorously not proportional to $\varepsilon_2(\vec{q},\omega)$ but, in fact, proportional to the loss function $\mathrm{Im}[-1/\varepsilon(\vec{q},\omega)]=\varepsilon_2(\vec{q},\omega)/[\varepsilon_1(\vec{q},\omega)^2+\varepsilon_2(\vec{q},\omega)^2]$.[1] Since most *K* edges are situated far above 100 eV, $\varepsilon_1(\vec{q},\omega)$ is usually very close to 1 while $\varepsilon_2(\vec{q},\omega)$ is

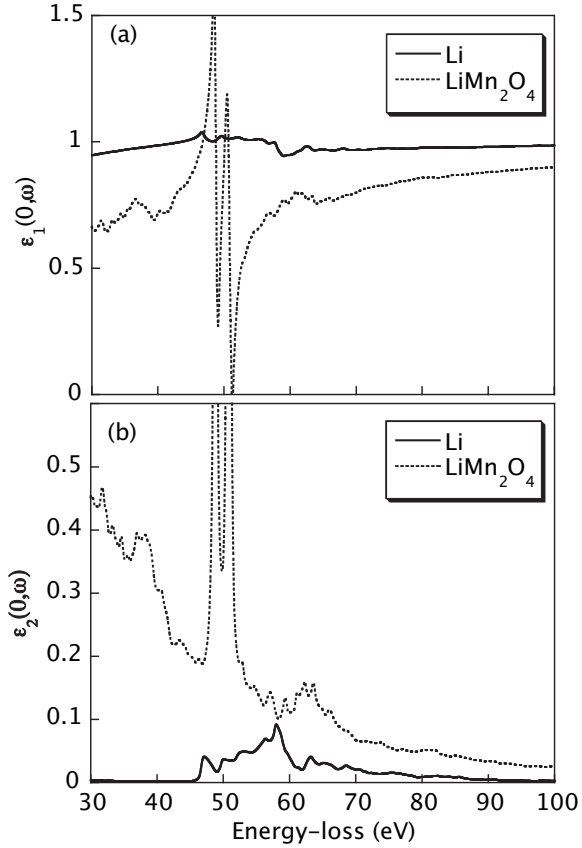

FIG. 9. (a) Real part and (b) imaginary part of the dielectric function, $\varepsilon(0,\omega)$, calculated for Li (full line) and for $LiMn_2O_4$ (dotted line), using the OPTIC program.

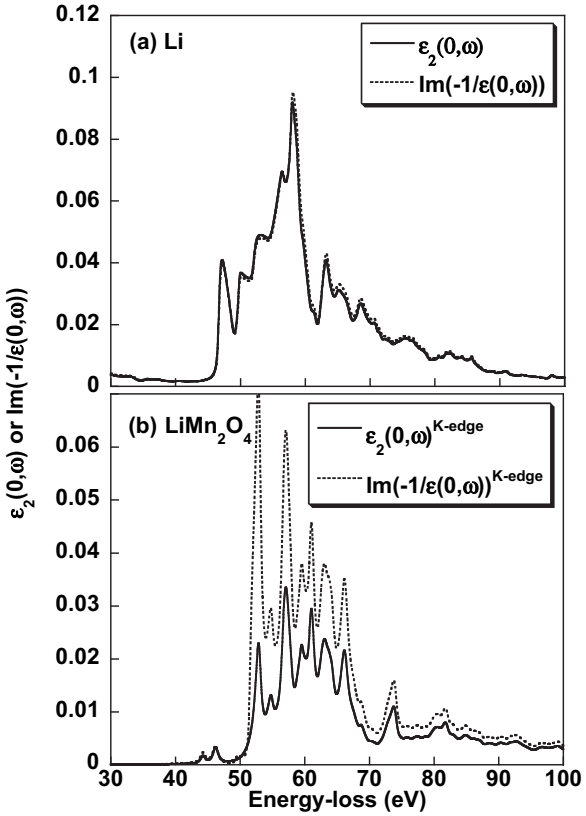

FIG. 10. Calculated Li K edges, using the OPTIC program, in the case of (a) Li, and (b) $LiMn_2O_4$. Full line: only considering $\varepsilon_2(0,\omega)$; dotted line: considering the loss function $\mathrm{Im}[-1/\varepsilon(0,\omega)]$.

very close to zero: their limit values at high energy. For these edges and to a good level of approximation, the loss function can consequently be taken as equal to $\varepsilon_2(\vec{q},\omega)$, which is precisely proportional to the DFF. On the contrary, since the Li K edge lies around 60 eV, neglecting polarization effects [taking $\varepsilon_1(\vec{q},\omega)\approx 1$] can be too much of an approximation and, in the calculation of the Li K edge, one should consider correcting $\varepsilon_2(\vec{q},\omega)$ by using the quantity $1/(\varepsilon_1^2+\varepsilon_2^2)$. This correction term (CT) will deviate from 1 as soon as there is a substantial increase in polarization effects. We have calculated the Li K edge in Li and $LiMn_2O_4$ and results concerning both real and imaginary parts of $\varepsilon(0,\omega)$ are given in Fig. 9(a) and 9(b), respectively. In the case of Li metal, the approximation of assimilating the loss function to $\varepsilon_2(\vec{q},\omega)$ is justified. $\varepsilon_2(0,\omega)$ is very close to zero before the edge onset and there are few, if any, polarization effects leading to a $\varepsilon_1(0,\omega)$ very close to 1. On the other hand, $\varepsilon_1(0,\omega)$ calculated in the case of $LiMn_2O_4$ is far from being equal to 1 and $\varepsilon_2(0,\omega)$ is not small compared to $\varepsilon_1(0,\omega)$. Two resonances corresponding to transitions from the $3p$ to the $3d$ states of manganese (at 49 eV and 51.2 eV) cause $\varepsilon_1(0,\omega)$ to drop just before the Li K edge in this compound. These two excitations also appear as two strong peaks in the calculation of $\varepsilon_2(0,\omega)$. These large variations of $\varepsilon_1(0,\omega)$ should have an impact on the Li K edge simulations, and so in order to evaluate this effect, we compared the Li K edges obtained from $\mathrm{Im}[-1/\varepsilon(0,\omega)]$ and from $\varepsilon_2(0,\omega)$ for these two compounds using the OPTIC program. In Figs. 10(a) and 10(b), results are shown for Li and $LiMn_2O_4$, respectively. In the case of Li metal, as was previously deduced from the examination of $\varepsilon_1(0,\omega)$ and $\varepsilon_2(0,\omega)$, both quantities are clearly equivalent. Polarization effects can safely be neglected in its EELS spectrum. In the case of $LiMn_2O_4$, the comparison was made difficult due to the presence of the Mn $M_{2,3}$ edge just before the Li K edge. So in order to correctly extract the Li K edge intensity, another matrix element calculation was performed introducing only the transitions between the $1s$ Li state and the conduction band. This is how we obtained the Li K edge given in Fig. 10(b) [labeled $\varepsilon_2(0,\omega)^{K\ \mathrm{edge}}$ and shown previously in Fig. 8]. This calculation is justified since, in the RPA and without LFE, $\varepsilon_2(0,\omega)$ is a sum over independent transitions. The following equation can be written:

$$\mathrm{Im}\left(\frac{-1}{\varepsilon(0,\omega)}\right)=\frac{\varepsilon_2(0,\omega)}{[\varepsilon_1(0,\omega)^2+\varepsilon_2(0,\omega)^2]}=\frac{1}{[\varepsilon_1(0,\omega)^2+\varepsilon_2(0,\omega)^2]}\times[\varepsilon_2(0,\omega)^{K\ \mathrm{edge}}+\varepsilon_2(0,\omega)^{\mathrm{other}}],\qquad(4)$$

where $\varepsilon_2^{\mathrm{other}}$ corresponds to all the transitions from the valence band to the conduction band, except that including the

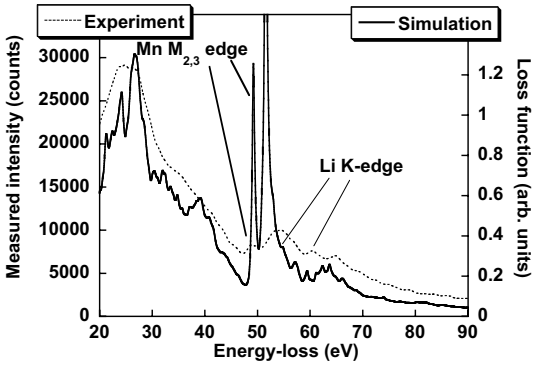

FIG. 11. Dotted line: experimental spectrum for $LiMn_2O_4$; full line: calculated loss function for $LiMn_2O_4$.

Li 1*s* state. Polarization effects on the Li *K* edge can thus be evaluated by applying the CT on the partial $\varepsilon_2(0,\omega)^{K\ \mathrm{edge}}$ contribution. The $\mathrm{Im}[-1/\varepsilon(0,\omega)]^{K\ \mathrm{edge}}$ obtained in this way corresponds to the sole Li *K* edge, including polarization effects stemming from the presence of the Mn $M_{2,3}$ edge. Even if peak positions are unchanged [Fig. 10(b)] due to the use of identical eigenvalues, the CT dramatically modifies relative peak intensities. Around 55 eV, relative intensities are increased by a factor of three when polarization effects are included. The introduced correction, however, worsens the correlation between the simulation and the experiment. This points to the fact that some important issues still need to be addressed.

First of all, the Li *K* edge is calculated to be 6 eV too close to the manganese $M_{2,3}$ edge (Fig. 11), in a region where the $\varepsilon_1(0,\omega)$ variations are extreme. Had the Li *K* edge been found to be 6 eV higher in energy, the effect of CT would have been much subtler. This point could be improved by correcting the Kohn-Sham energies with a calculation using the GW approximation.[49] The Li *K* edge would thus be calculated in an energy range where corrections would be more realistic. Second, since LFE are not taken into account, the intensity of the manganese $M_{2,3}$ edge is overestimated (Fig. 11). The inclusion of these effects was shown to improve the simulation of the titanium $M_{2,3}$ edge in TiO_2, by considerably lowering its intensity.[50] In our case, such effects are indeed present to a great extent. Calculations involving LFE are in progress and will be detailed in a forthcoming paper.

In spite of these approximations, our results show that polarization effects can be important if a transition metal $M_{2,3}$ edge is present just before the Li *K* edge, all the more so as one progresses to the right of the periodic table (from Ti to Co, Ni, …). We consequently expect Li *K* edges in iron (for example: $LiFePO_4$) or cobalt (for example: $LiCoO_2$) based materials to be very sensitive to these effects.

VI. CONCLUSION

We described different methods that allow the calculation of the Li *K* edge in various compounds, and particularly in those present in lithium batteries. It was shown that treating the 1*s* level as a core or a valence level in the self-consistent calculation of the electronic density did not significantly affect the resulting ELNES spectra. We thus conclude that the simplest calculation (with the 1*s* level as a core level) is sufficient. It was also shown that monopolar terms were important when using the DFF approach but that their removal led to consistent spectra. For the same set of parameters, the approaches based on the calculation of the DFF or of the dielectric function gave identical spectra demonstrating that the orthogonalization of the wave function does not constitute a major problem in the Li *K* edge simulation. The muffin tin radius choices were shown to modify the relative intensities of peaks that are far apart from one another. This represents one of the largest uncertainties in the intensities of the simulations.

Based on three model compounds, it was proven that simulations of the Li *K* edges are in very good agreement with experimental observations. The importance of the core-hole effects were demonstrated on Li_2O and shown to depend on the energy range considered in the spectrum. Using a partial core-hole in order to simulate a partial screening could also be a way to improve the simulation.

The main results stem, however, from the discussion of the approximation $\mathrm{Im}[-1/\varepsilon(0,\omega)]=\varepsilon_2(0,\omega)$. In the case of small polarization effects, i.e., ε_1 close to one (Li metal), this approximation was shown to be justified. In the case of $LiMn_2O_4$, the presence of the $M_{2,3}$ edge creates a large polarization which greatly modifies the simulated spectrum. In this case, the full dielectric function must be calculated. In order to completely simulate the low-loss spectrum, it is however essential to take into account proper Kohn-Sham energies in order to position correctly the $M_{2,3}$ and *K* edges (using a GW approximation). LFE also have to be included. Such improved calculations will allow for the determination of accurate intensities for both the transition metal edge and the lithium edge and may well serve to ascertain the lithium content in lithium battery materials.

ACKNOWLEDGMENTS

The computations presented in this work were performed at the "Centre Régional de Calcul Intensif des Pays de la Loire" financed by the French Research Ministry, the "Région Pays de la Loire," and the University of Nantes.

[1] R. F. Egerton, *Electron Energy-Loss Spectroscopy in the Electron Microscope*, 2nd edition (Plenum Press, New York, 1996).
[2] M. Knupfer and J. Fink, Synth. Met. **141**, 21 (2004).
[3] A. Marini, R. Del Sole, and A. Rubio, Phys. Rev. Lett. **91**, 256402 (2003).
[4] M. Launay, F. Boucher, and P. Moreau, Phys. Rev. B **69**, 035101 (2004).
[5] B. Rafferty and L. M. Brown, Phys. Rev. B **58**, 10326 (1998).
[6] M. C. Cheynet and R. Pantel, Micron **37**, 377 (2006).
[7] P. Moreau, N. Brun, C. A. Walsh, C. Colliex, and A. Howie, Phys. Rev. B **56**, 6774 (1997).
[8] M. Varela, S. D. Findlay, A. R. Lupini, H. M. Christen, A. Y. Borisevich, N. Dellby, O. L. Krivanek, P. D. Nellist, M. P. Oxley, L. J. Allen, and S. J. Pennycook, Phys. Rev. Lett. **92**, 095502 (2004).
[9] K. Lie, R. Brydson, and H. Davock, Phys. Rev. B **59**, 5361 (1999).
[10] A. Gloter, V. Serin, C. Turquat, C. Cesari, C. Leroux, and G. Nihoul, Eur. Phys. J. D **22**, 179 (2001).
[11] J. Tafto and O. L. Krivanek, Phys. Rev. Lett. **48**, 560 (1982).
[12] D. H. Pearson, C. C. Ahn, and B. Fultz, Phys. Rev. B **47**, 8471 (1993).
[13] L. Laffont, M. Y. Wu, F. Chevallier, P. Poizot, M. Morcrette and J. M. Tarascon, Micron **37**, 459 (2006).
[14] G. Xu X., C. Li, J. X. Li, U. Kolb, F. Wu, and G. Chen, J. Phys. Chem. B **107**, 11648 (2003).
[15] J. Graetz, C. C. Ahn, R. Yazami, and B. Fultz, J. Phys. Chem. B **107**, 2887 (2003).
[16] A. Hightower, C. C. Ahn, B. Fultz, and P. Rez, Appl. Phys. Lett. **77**, 238 (2000).
[17] R. F. Egerton, P. Li, and M. Malac, Micron **35**, 399 (2004).
[18] Y. Shiraishi, I. Nakai, K. Kimoto, and Y. Matsui, J. Power Sources **97-98**, 461 (2001).
[19] Young-Gu Jin and K. J. Chang, Phys. Rev. B **59**, 14841 (1999).
[20] K. Sturm and L. E. Oliveira, Phys. Rev. B **40**, 3672 (1989).
[21] K. Karlsson and F. Aryasetiawan, Phys. Rev. B **52**, 4823 (1995).
[22] R. Brydson, J. Bruley, and J. M. Thomas, Chem. Phys. Lett. **149**, 343 (1988).
[23] N. Jiang and J. C. H. Spence, Phys. Rev. B **69**, 115112 (2004).
[24] P. Blaha, K. Schwarz, G. K. H. Madsen, D. Kvaniscka, and J. Luitz, WIEN2K, An Augmented Plane Wave+Local Orbitals Program for Calculating Crystal Properties, edited by K. Schwarz (Techn. Universität Wien, Austria, 2001).
[25] D. J. Singh, *Planewaves, Pseudopotentiels and the LAPW Method* (Kluwer Academic Publishers, London, 1994).
[26] S. Cottenier, Density Functional Theory and the Family of (L)APW-methods: a step-by-step introduction (Instituut voor Kern- en Stralingsfysica, K.U. Leuven, Belgium 2002).
[27] P. Hohenberg and W. Kohn, Phys. Rev. **136**, B864 (1964).
[28] W. Kohn and L. J. Sham, Phys. Rev. **140**, A1133 (1965).
[29] M. Inokuti, Rev. Mod. Phys. **43**, 297 (1971).
[30] C. Ambrosch-Draxl and J. O. Sofo, cond-mat/0402523 (unpublished).
[31] D.-R. Liu, H. E. George Rommal and D. B. Williams, J. Electron Microsc. Tech. **4**, 381 (1986).
[32] P. Fallon and C. A. Walsh, Computer Code PEELS, University of Cambridge, England 1996.
[33] R. F. Egerton and M. Malac, Ultramicroscopy **92**, 47 (2002).
[34] A. P. Stephen's, Ph D Thesis, University of Cambridge, Cambridge, England, 1980.
[35] J. P. Perdew, K. Burke and M. Ernzerhof, Phys. Rev. Lett. **77**, 3865 (1996).
[36] J. C. Slater, Phys. Rev. **51**, 151 (1937).
[37] D. Singh, Phys. Rev. B **43**, 6388 (1991).
[38] D. Pines and P. Nozières, *The Theory of Quantum Liquids* (Addison-Wesley Publishing Company, 1989), Vol. 1.
[39] P. Schattschneider, M. Nelhiebel, H. Souchay, and B. Jouffrey, Micron **31**, 333 (2000).
[40] L. J. Allen, S. D. Findlay, M. P. Oxley, C. Witte, and N. J. Zaluzec, Phys. Rev. B **73**, 094104 (2006).
[41] M. Nelhiebel, P.-H. Louf, P. Schattschneider, P. Blaha, K. Schwarz, and B. Jouffrey, Phys. Rev. B **59**, 12807 (1999).
[42] P. Moreau, F. Boucher, G. Goglio, D. Foy, V. Mauchamp, and G. Ouvrard, Phys. Rev. B **73**, 195111 (2006).
[43] C. Hébert, J. Luitz, and P. Schattschneider, Micron **34**, 219 (2003).
[44] C. Hébert-Souche, P.-H Louf, P. Blaha, M. Nelhieble, J. Luitz, P. Schattschneider, K. Schwarz, and B. Jouffrey, Ultramicroscopy **83**, 9 (2000).
[45] C. Elsässer and S. Köstlmeier, Ultramicroscopy **86**, 325 (2001).
[46] Y. Ishii, J. Murakani, and M. Itoh, J. Phys. Soc. Jpn. **68**, 696 (1999).
[47] G. Onida, L. Reining, and A. Rubio, Rev. Mod. Phys. **74**, 601 (2002).
[48] D. R. Hamann and D. A. Muller, Phys. Rev. Lett. **89**, 126404 (2002).
[49] L. Hedin, Phys. Rev. **139**, A796 (1965).
[50] N. Vast, L. Reining, V. Olevano, P. Schattschneider, and B. Jouffrey, Phys. Rev. Lett. **88**, 037601 (2002).